Spectra of $W^{19+}-W^{32+}$ observed in the EUV region between 15 and 55 Å with an electron-beam ion trap

H. A. Sakaue,[1] D. Kato,[1,2] N. Yamamoto,[3] N. Nakamura,[4] and I. Murakami[1,2]

[1]*National Institute for Fusion Science, Toki, Gifu 509-5292, Japan*

[2]*Department of Fusion Science, SOKENDAI (The Graduate University for Advanced Studies), Toki, Gifu 509-5292, Japan*

[3]*Chubu University, Kasugai, Aichi 487-8501, Japan*

[4]*Institute for Laser Science, The University of Electro-Communications, Chofu, Tokyo 182-8585, Japan*

(Received 19 April 2015; published 6 July 2015)

We present extreme ultraviolet spectra of highly charged tungsten ions ($W^{19+}-W^{32+}$) in the wavelength range of 15−55 Å obtained with a compact electron-beam ion trap (CoBIT) and a grazing-incidence spectrometer at the National Institute for Fusion Science. The electron energy dependence of the spectra was investigated for electron energies from 490 to 1320 eV. Identification of the observed lines was aided by collisional-radiative (CR) modeling of CoBIT plasma. Good quantitative agreement was obtained between the CR-modeling results and the experimental observations. The ion charge dependence of the $6g$-$4f$, $5g$-$4f$, $5f$-$4d$, $5p$-$4d$, and $4f$-$4d$ transition wavelengths were measured.

DOI: 10.1103/PhysRevA.92.012504 PACS number(s): 32.30.−r, 34.50.Fa, 34.10.+x, 52.20.Fs

I. INTRODUCTION

Tungsten is planned to be used as material for the divertor plates in the International Thermonuclear Experimental Reactor (ITER) because of the high sputtering threshold energy for light ion bombardment, the highest melting point among all the elements, and the lower tritium retention compared with carbon-based materials. Since in ITER extremely high particle flux and heat flux are predicted based on the intermittent edge plasma transport, for example, the edge-localized mode, fluxes cause serious damage to such components, tungsten is therefore considered to be one of the most abundant impurities in the ITER plasma. However, impurity tungsten enters the high-temperature plasma and is ionized to highly charged ions, and highly charged ions then emit very strong photons of EUV and/or x rays. These photons have very important information on plasma diagnostics and information on electron and ion temperatures, electron density, impurity ion abundance, and impurity transportation. The impurity tungsten exists not only in the core region of high-temperature plasma, but also in the plasma area of the relatively low temperature of the divertor vicinity. The energy range of the plasma in which there are highly charged impurity tungsten ions in the fusion reactor, such as ITER, becomes extensive from several tens eV to several tens keV. The charge states of highly charged tungsten ions existing in such plasma are from approximately several tens to about 60, and it is in the present conditions that those emission spectra are very complicated and those spectral data are very poor. Emission lines of highly charged tungsten ions thus play an important role in the spectroscopic diagnostics of the ITER plasma. Consequently, the spectroscopic data of tungsten ions have been studied at several facilities [1–3]. An electron-beam ion trap is a useful device for the systematic spectroscopic studies of highly charged tungsten ions [4–7]. We have constructed a compact electron-beam ion trap called CoBIT for spectroscopic studies of moderate charge state ions [8–12]. In this paper, we present EUV spectra obtained with the electron energy range of 490–1320 eV. To identify the observed lines, we have calculated the spectra using a collisional-radiative model. From the comparison, some observed lines have been identified as the $6g$-$4f$, $5f$-$4d$, $5p$-$4d$, and 4-4d transitions of $W^{19+}-W^{32+}$.

II. EXPERIMENT

The experimental apparatus consists of CoBIT, which is a highly charged ion source, and an EUV spectrometer. CoBIT mainly consists of an electron gun, an ion trap (drift tube), an electron collector, a superconducting coil, and a liquid-nitrogen tank [8]. The high critical temperature superconducting Helmholtz coils, which can be used at the liquid-nitrogen temperature, are mounted around the drift tube. The electron beam emitted from the electron gun is accelerated (or decelerated) toward the drift tube and compressed by the magnetic field produced by the superconducting Helmholtz coil. After passing through the drift tube, the electron beam is collected by the electron collector. All the electrodes in CoBIT are fixed in the liquid-nitrogen tank with ceramic insulators (Shapal M-soft), which have a high thermal conductivity to keep them at low temperatures. The electron collector, at which 10 W is consumed at the maximum, is also cooled through this thermal conductivity. Tungsten was injected into CoBIT as vapor of tungsten hexacarbonyl $W(CO)_6$ through a gas injection system and ionized at the center of CoBIT. We developed a slitless EUV spectrometer of CoBIT. In general, it is necessary to install an entrance slit in front of a diffraction grating, but we designed the spectrometer of the slitless type because an electron-beam ion trap (EBIT) represents a line source with a width of several hundred micrometers. Therefore, highly efficient spectroscopic measurement became possible. The designed spectrometer is a flat-field grazing-incidence (87°) spectrometer with a 2400 grooves/mm laminar-type replica diffraction grating (30-003, Shimadzu Corporation). A backilluminated extreme ultraviolet sensitive charge-coupled device (CCD) detector was mounted at the focal position. The CCD is movable on the focusing plane. The size of the CCD is $26.8 \times 8.0\,\mathrm{mm}^2$ with a pixel size of $20 \times 20\ \mu\mathrm{m}^2$ and the number of channels of 1340×400. The available wavelength range is from 10 to 55 Å with this grating. The stray visible

light from the cathode of the electron gun was filtered out by an aluminum foil (0.15 μm thickness) placed in front of the CCD. The transmittance of the aluminum EUV filter is over 80% around 20 Å. However, it is rapidly decreased from 20 Å, and it almost becomes 0 at 70 Å. Therefore, it is necessary to correct the transmittance of the spectrometer. The intensity of the experimental spectra was corrected with the efficiency obtained from the product of the following three components: (i) the transmittance of the aluminum filter calculated assuming that the filter is pure aluminum, (ii) the reflectivity of grating supplied from the company, and (iii) the quantum efficiency and gain of the CCD given in the product catalog.

A wavelength of tungsten spectra was calibrated by emission lines of Fe XVII $2p$-$3d$ and $2p$-$3s$ transitions with wavelengths taken from the NIST Atomic Spectra Database (ASD). For the calibration spectra, iron was injected into CoBIT plasma as the vapor of ferrocene [$Fe(C_5H_5)_2$] through a gas injection system.

III. COLLISIONAL-RADIATIVE MODEL

In order to examine measured spectra, we have constructed a CR model for W^{19+}–W^{32+} ions. Fine-structure levels with principal quantum number n up to 6 were considered. For W^{19+}–W^{27+} ions, $4p^64d^{10}4f^a (a = 1–9)$, $4p^64d^{10}4f^{a-1}nl$ ($n = 5,6$ and $l = 0–4$), and $4p^64d^94f^{a+1}$ configurations were considered. For W^{28+}–W^{32+} ions, $4p^64d^a$ ($a = 6–10$), $4p^64d^{a-1}4f$, $4p^64d^{a-1}nl$ ($n = 5,6$ and $l = 0–4$), $4p^64d^{a-2}4f^2$, $4p^54d^{a+1}$, and $4p^54d^a4f$ configurations were considered. In addition to the above configurations, we include more configurations for W^{27+}-W^{29+} ions to obtain better wavelengths to compare with measurements in CoBIT for the shorter wavelength region: $4p^54d^{10}4f^2$, $4p^64d^{10}nl$ (n up to 8 and $l = 0–4$), and $4p^64d^94fnl$ ($n = 5,6$ and $l = 0–4$) for W^{27+}; $4p^54d^94f^2$, $4p^64d^9nl$ (n up to 8 and $l = 0–4$), $4p^54d^{10}nl$ ($n = 5,6$ and $l = 0–4$), and $4p^64d^84f5l$ ($l = 0–4$) for W^{28+}; and $4p^54d^84f^2$, $4p^64d^8nl$ (n up to 8 and $l = 0–4$), p^54d^9nl ($n = 5,6$ and $l = 0–4$), and $4p^64d^74f5l$ ($l = 0–4$) for W^{29+}. Energy levels, radiative transition probabilities, electron-impact excitation, and ionization cross sections were calculated by the HULLAC atomic code [13]. Atomic structure was calculated using a parametric potential method. The electron-impact excitation and ionization cross sections were calculated by relativistic distorted-wave approximation. Electron-impact excitation and ionization rate coefficients were calculated with a monoenergetic electron energy represented by a Dirac Δ function in the range of 490 − 1320 eV. The population densities of excited levels and the spectral line intensities for each ion were obtained by solving the rate equations for the excited levels under a quasi-steady-state assumption. Radiative decay and electron-impact excitation and ionization processes among excited levels were taken into account in the rate equations. Recombination processes were ignored because in CoBIT excited levels of each ion were assumed to be populated mainly by electron-impact excitation from the ground state. Electron density was assumed as 10^{10} cm^{-3}, which is a typical density in CoBIT.

Ion charge state distribution in CoBIT was not calculated with the CR model since we do not consider the recombination rate coefficients for these tungsten ions here. Instead, we estimated the ion charge state distribution by fitting the measured spectra with synthesized spectra using the spectral line intensities calculated by the CR model as described below.

IV. RESULTS AND DISCUSSION

Figure 1 shows the EUV spectra at electron energies (E_e) between 490 and 1320 eV in the wavelength range of 15–55 Å. Parts of the spectra are also shown on an expanded scale with the scale multipliers identified in the figure.

In experiment, the electron energy (E_e) of CoBIT is set as follows:

$$I_p(q) < E_e(q) < I_p(q+1),$$

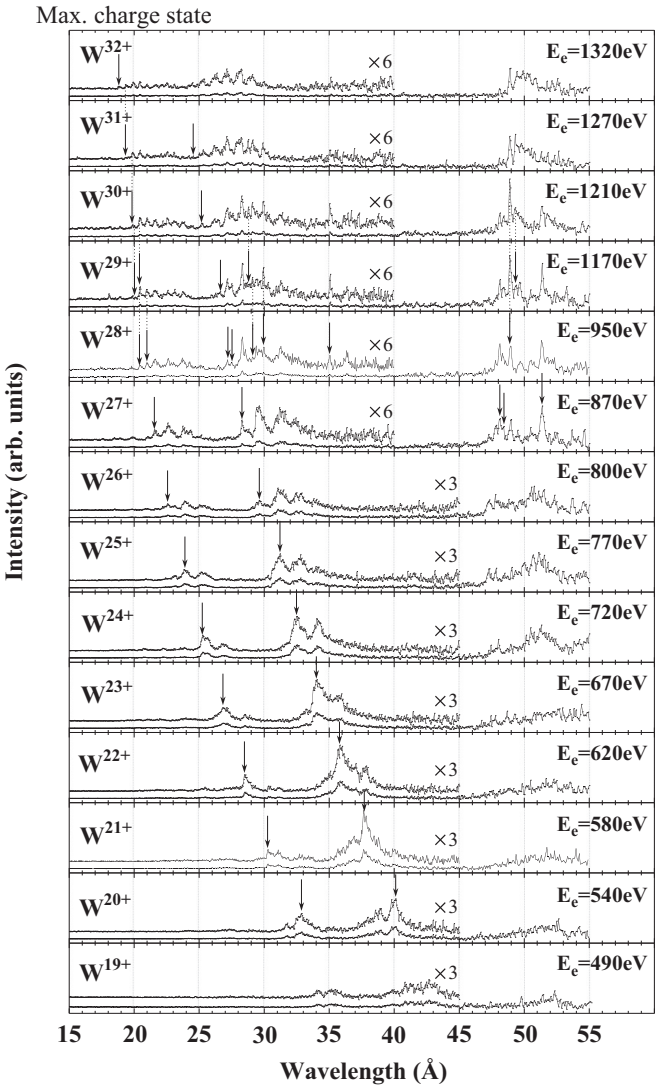

FIG. 1. EUV spectra of highly charged tungsten ions obtained at electron energy E_e from 490 to 1320 eV in the wavelength range of 15–55 Å. The peaks denoted by arrows were identified from comparison with the CR model. "Max. charge state" means the highest charge state of tungsten ions which can be produced in CoBIT at electron energy E_e.

where $I_p(q)$ is the ionization energy of the highly charged tungsten ion $W^{q+}(q = 19–32)$ [14]. Under these conditions, the maximum charge state (indicated as Max. charge state in the figure) at $E_e(q)$ should be q. Thus, the line that appeared when the energy was increased from $E_e(q-1)$ to $E_e(q)$ can be considered to be an emission line from W^{q+}. For example, lines at 26.8 and 34.0 Å observed in the spectrum at $E_e = 670$ eV can be identified as emissions from W^{23+} since they could not be observed below the ionization energy of W^{22+} (641 eV) and appeared just above the ionization energy. However, as the charge state is increased, the emission from the maximum charge state becomes weaker since the abundance of the maximum charge state becomes smaller due to a small ionization cross section and a large charge exchange cross section. Thus, careful adjustment of the injection gas pressure is important to maintain a narrow charge state distribution especially at higher electron energies. The spectra shown in Fig. 1 were taken after finding the best experimental condition for the injection gas pressure. Thus a narrow charge state distribution that contains only three to four charge states was realized. This procedure is important for making reliable identifications.

The emission lines of these spectra in Fig. 1 can be divided into two groups. One group is emission lines in the range of 15–45 Å, and the other group is emission lines in the range of 45–55 Å. As seen in the figure, the EUV spectra in the range of 15–45 Å show significant dependence on the electron energy [15]. As the electron energy and the ion charge state increase, the wavelength of strong emission lines shifts to a shorter wavelength region. Since the amount of the wavelength shift gradually becomes smaller as the electron energy increases, emission lines of different charge states fall into the narrow wavelength region (25–30 Å). On the other hand, the emission lines in the range of 45–55 Å were observed as broad lines over almost the entire energy range, and these emission line intensities are three to six times larger than that of the short-wavelength group. Unlike emission lines observed in the wavelength range of 15–45 Å, even if the charge state of highly charged tungsten ions is changed, the wavelength of this broad emission line group shifts slightly. The wavelength is almost constant at approximately the center wavelength 50 Å.

In Figs. 2 and 3, the typical EUV spectra are shown at electron energy $E_e = 800$ and 1210 eV in CoBIT, respectively, with the synthesized spectra from the CR model in the range of 15–45 Å. The top panel shows calculated spectra for each ion by the CR model. The middle panel is the synthesized spectrum from calculations. The bottom panel is the experimentally measured spectrum of CoBIT. CR-model spectra are convoluted with approximately 0.06-Å full width at half maximum to match the experimental spectra. Ion abundance was estimated by fitting the CR-model line spectra to experimentally measured spectra. The obtained ion abundance is indicated in Figs. 2 and 3. The CR-model spectra agree with the experimental spectra very well. Based on the comparison with the model spectra and the energy dependence of the spectra (Fig. 1), emission lines from the $6g$-$4f$ and $5g$-$4f$ transitions for W^{24-26+} are identified as shown by the arrows in Fig. 2. Each peak is the group of emission lines due to fine-structure transitions of the same

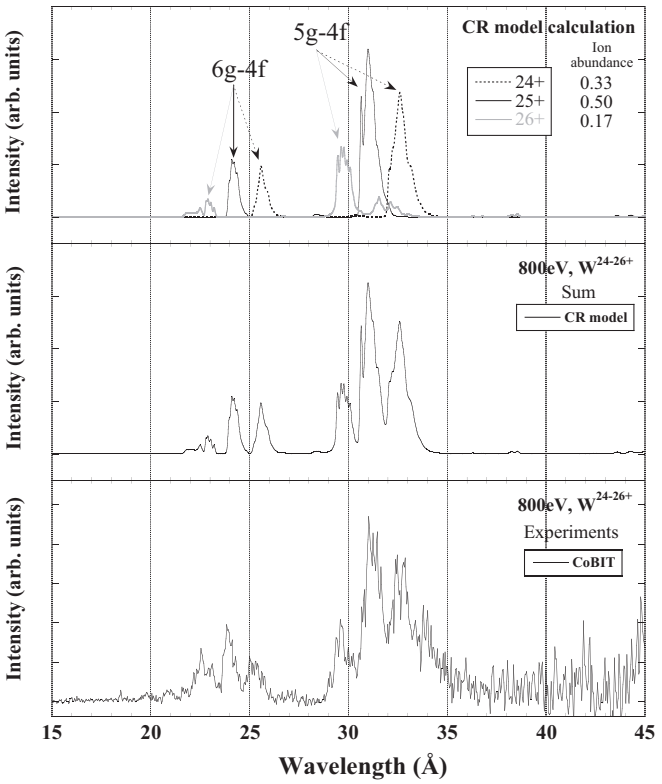

FIG. 2. Experimental spectra in CoBIT and calculated spectra of the CR model at electron energy $E_e = 800$ eV in the range of 15–45 Å. The top panel is the CR-model calculation spectrum. The middle panel is the sum of these spectra. The bottom panel is the experimentally measured spectrum of CoBIT.

electron configurations. When the ion charge q is lower than 28+ since the $4d$ shell is closed in the ground state and the $4f$ shell is the valence shell, the emission lines from the ng-$4f$ transitions are dominant. For the spectrum at 1210 eV (Fig. 3), emission lines from the $5f$-$4d$, $6g$-$4f$, $5g$-$4f$, and $5p$-$4d$ transitions for W^{26-29+} are identified as shown by the arrows based on the comparison with the model spectra and the energy dependence. When the ion charge q is 28+ or higher, the $4f$ shell becomes empty in the ground states. Thus, the ng-$4f(n = 5,6)$ transition lines become weaker. The $5f$-$4d$ and $5p$-$4d$ transitions become dominant instead of the $6g$-$4f$ and $5g$-$4f$ transitions because these transitions are no longer the inner-shell excitation transitions. Table I shows the identified transitions labeled by both LS and jj schemes and the wavelengths of these emission lines. The total error of the wavelength is ±0.01 Å (calibration error and fitting error, respectively, are approximately ±0.01 Å). The fine structure was identified. This table also includes other experimental and calculated wavelengths [2,16–18]. These eight lines are sharp in comparison with other emission lines from the low charge states in Fig. 2 because the electron configurations of these transitions are simple systems which have one valence electron or vacancy or closed shell (Ag-like, Pd-like, and Rh-like ions).

Similar to the above example, based on the comparison with the model and the experimental energy dependence, emission lines from W^{19+} to W^{32+} have been identified for the spectra obtained at electron energies of 490–1320 eV as shown by

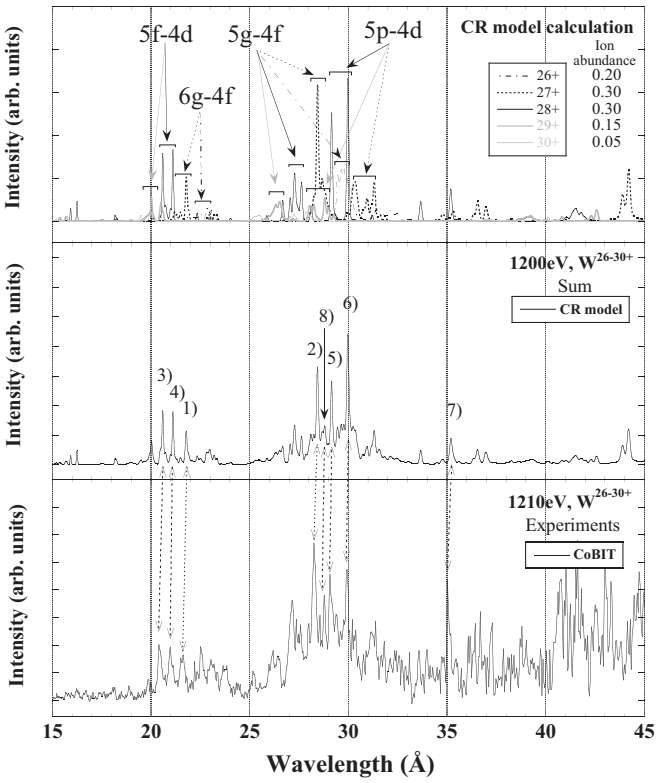

FIG. 3. Experimental spectra in CoBIT and calculated spectra of the CR model at electron energy $E_e = 1210$ and 1200 eV in the range of 15−45 Å, respectively. The transition and wavelength of the lines labeled by numbers are shown in Table I.

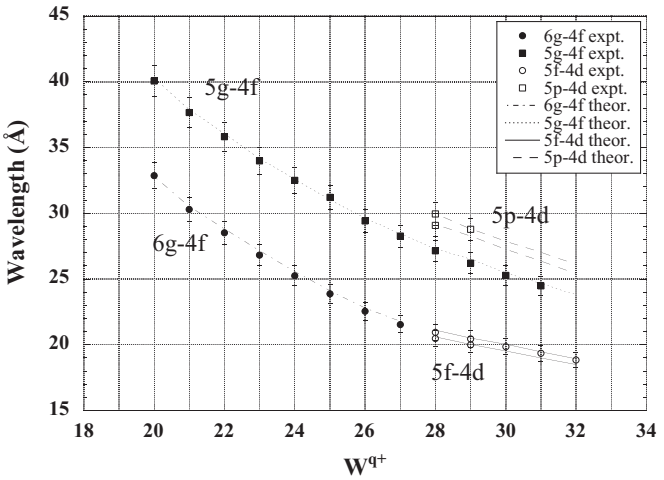

FIG. 4. The charge dependence of the wavelength for each emission line. A circle, an open circle, a square, and an open square are the experimental values corresponding to the $6g$-$4f$, $5f$-$4d$, $5g$-$4f$, and $5p$-$4d$ lines, respectively. The dot-dashed line, dotted line, two-dot-dashed line, and dashed line, respectively, are the calculated wavelengths corresponding to the same transitions array in the above by our CR model.

the arrows in Fig. 1 (the lines identified as a transition from the ion with the Max. charge state are shown by arrows in Fig. 1). Figure 4 shows the charge state dependence of the wavelengths for those emission lines. The charge dependence of the CR-model calculation at the nl-$4l'$ transitions agrees with that of the experimental value very well. The differences between calculated value and experimental value are less than

TABLE I. Transition and wavelength of Ag-like, Pd-like, and Rh-like tungsten ions.

			Transition		Expt. (Å)		Theor. (Å)	
Line number	Ion		Upper	Lower	Present	Previous	Present	Previous
(1)	Ag-like W^{27+}	nl, LSJ	$4d^{10}6g\ ^2G_{7/2}$	$\rightarrow 4d^{10}4f\ ^2F_{5/2}$	21.62		21.75	21.66[b]
		$(nl, jj$	$4d^4_{3/2}4d^6_{5/2}6g^1_{7/2}J = 7/2$	$\rightarrow 4d^4_{3/2}4d^6_{5/2}4f^1_{5/2}J = 5/2)$				
(2)	Ag-like W^{27+}	nl, LSJ	$4d^{10}5g\ ^2G_{7/2}$	$\rightarrow 4d^{10}4f\ ^2F_{5/2}$	28.31		28.45	28.33[c]
		$(nl, jj$	$4d^4_{3/2}4d^6_{5/2}5g^1_{7/2}J = 7/2$	$\rightarrow 4d^4_{3/2}4d^6_{5/2}4f^1_{5/2}J = 5/2)$				
(3)	Pd-like W^{28+}	nl, LSJ	$4d^95f\ ^1P_1$	$\rightarrow 4d^{10}\ ^1S_0$	20.44		20.56	20.81[d]
		$(nl, jj$	$4d^3_{3/2}4d^6_{5/2}5f^1_{5/2}J = 1$	$\rightarrow 4d^4_{3/2}4d^6_{5/2}J = 0)$				
(4)	Pd-like W^{28+}	nl, LSJ	$4d^95f\ ^3P_1$	$\rightarrow 4d^{10}\ ^1S_0$	20.95		21.07	21.44[d]
		$(nl, jj$	$4d^4_{3/2}4d^5_{5/2}5f^1_{7/2}J = 1$	$\rightarrow 4d^4_{3/2}4d^6_{5/2}J = 0)$				
(5)	Pd-like W^{28+}	nl, LSJ	$4d^95p\ ^1P_1$	$\rightarrow 4d^{10}\ ^1S_0$	29.09	29.51[a]	29.07	29.345[d]
		$(nl, jj$	$4d^4_{3/2}4d^5_{5/2}5p^1_{1/2}J = 1$	$\rightarrow 4d^4_{3/2}4d^6_{5/2}J = 0)$				
(6)	Pd-like W^{28+}	nl, LSJ	$4d^95p\ ^3P_1$	$\rightarrow 4d^{10}\ ^1S_0$	29.93		29.88	30.221[d]
		$(nl, jj$	$4d^3_{3/2}4d^6_{5/2}5p^1_{1/2}J = 1$	$\rightarrow 4d^4_{3/2}4d^6_{5/2}J = 0)$				
(7)	Pd-like W^{28+}	nl, LSJ	$4d^95sJ = 2$	$\rightarrow 4d^{10}\ ^1S_0$	35.05		35.07	
		$(nl, jj$	$4d^4_{3/2}4d^5_{5/2}5s^1_0J = 2$	$\rightarrow 4d^4_{3/2}4d^6_{5/2}J = 0)$				
(8)	Rh-like W^{29+}	nl, LSJ	$4d^85pJ = 7/2$	$\rightarrow 4d^94fJ = 5/2$	28.79		28.71	
		$(nl, jj$	$4d^3_{3/2}4d^5_{5/2}5p^1_{1/2}J = 7/2$	$\rightarrow 4d^4_{3/2}4d^5_{5/2}J = 5/2)$				

[a]Reference [2].
[b]Reference [16].
[c]Reference [17].
[d]Reference [18].

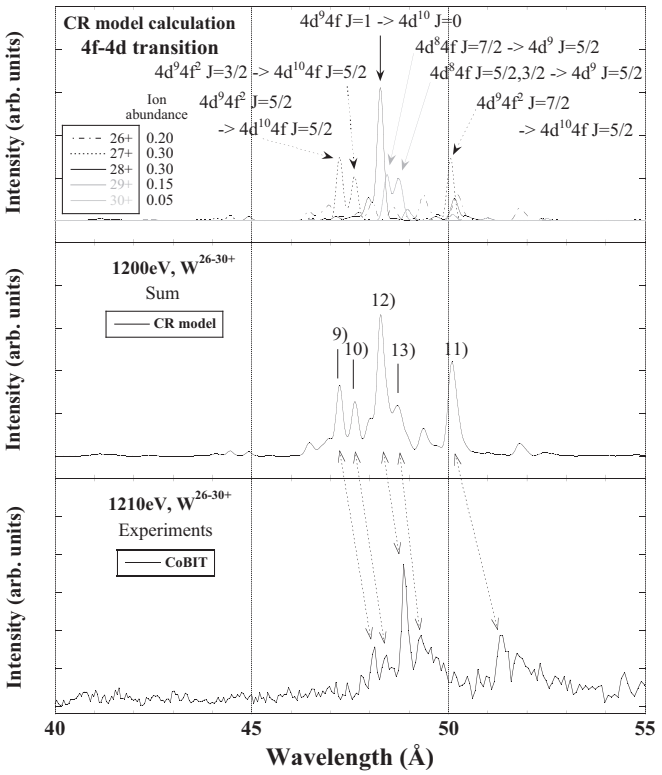

FIG. 5. Experimental spectra in CoBIT and calculated spectra of the CR model at electron energy $E_e = 1210$ and 1200 eV in the range of 40 – 55 Å, respectively. The transition and wavelength of these numbering lines are shown in Table II.

0.14 Å. The $6g$-$4f$ and $5g$-$4f$ transitions are dominant when the charge state is lower than 28+. When the ion charge q becomes higher than 28+, the emission lines corresponding to the $5f$-$4d$ and $5p$-$4d$ transitions, respectively, appear. The emission lines of the $5f$-$4d$ and $5p$-$4d$ transitions from W^{28+} show four strong peaks (3)–(6) reflecting on the spin-orbit splitting of $4d$, $5p$, and $5f$.

Harte *et al.* [19] observed EUV spectra from laser-produced tungsten plasma for the 10−70-Å ranges. Based on the comparison with the transition probability distribution calculated by the Hartree-Fock with the configuration interaction code of Cowan [20], they identified lines observed on broad continuum as $5f$-$4d$, $5p$-$4d$, and $5g$-$4f$ transitions of $W^{20+-37+}$ ions. They argue that the transition from a high-n, l state (such as a $6g$-$4f$ transition) would most likely be collisionally quenched in a dense plasma and so will not be significant. On the other hand, at the lower electron density plasma (such as CoBIT plasma) in comparison with laser-produced plasma, the emission lines of the $6g$-$4f$ transitions were observed and these transitions were dominant at charge states lower than W^{28+}. Similarly, in the large helical device (LHD) plasma, the emission lines of the $6g$-$4f$ transitions were observed [21]. Therefore, in the plasma of the electron density, such as the discharges in LHD, it is also necessary to consider high principal quantum number excited states in plasma modeling because experimental results suggest that there are transitions from high principal quantum number levels.

In Fig. 5, the typical EUV spectra are shown at electron energy $E_e = 1210$ eV in CoBIT with the synthesized spectra from the CR model at $E_e = 1200$ eV in the range of 40−55 Å. Top, middle, and bottom panels show CR-model calculated spectra for each ion, the synthesized spectrum, and the experimentally measured spectrum, respectively. The estimated ion abundance is indicated in the figure. As seen in the figure, the calculated wavelengths show a systematic shift of 0.5−1 Å when compared with the experimental wavelength. There would exist difficulties in achieving high accuracies in energy-level calculations for multielectron systems with the parametric potential method of the HULLAC atomic code, and such a difference in wavelengths for $n = 4$-4 transitions remains as uncertainties of the calculations. Nevertheless, the CR-model spectrum reproduces the experimental spectrum very well. These photons are emitted from the $4f$-$4d$ transitions. In a spectrum of 1210 eV, five sharp emission lines were observed. These are indicated by (9)–(13) in Fig. 5. These emission lines

TABLE II. $4d$-$4f$ transition and wavelength of Ag-like, Pd-like, and Rh-like tungsten ions.

					Expt. (Å)		Theor. (Å)	
Line number	Ion		Upper	Lower	Present	Previous	Present	Previous
(9)	Ag-like W^{27+}	nl, LSJ	$4d^9 4f^2\ ^2F_{5/2}$	$\rightarrow 4d^{10} 4f\ ^2F_{5/2}$	48.12	48.729[c]	47.22	48.555[c]
		$(nl, jj$	$4d^3_{3/2} 4d^6_{5/2} 4f^2_{5/2} J = 5/2$	$4d^4_{3/2} 4d^6_{5/2} 4f_{5/2} J = 5/2)$				
(10)	Ag-like W^{27+}	nl, LSJ	$4d^9 4f^2\ ^2D_{3/2}$	$\rightarrow 4d^{10} 4f\ ^2F_{5/2}$	48.40	49.403[c]	47.61	48.919[c]
		$(nl, jj$	$4d^3_{3/2} 4d^6_{5/2} 4f^2_{5/2} J = 3/2$	$4d^4_{3/2} 4d^6_{5/2} 4f_{5/2} J = 5/2)$		49.4[a]		
(11)	Ag-like W^{27+}	nl, LSJ	$4d^9 4f^2\ ^2G_{7/2}$	$\rightarrow 4d^{10} 4f\ ^2F_{5/2}$	51.39	51.457[c]	50.04	51.245[c]
		$(nl, jj$	$4d^3_{3/2} 4d^6_{5/2} 4f^2_{5/2} J = 7/2$	$4d^4_{3/2} 4d^6_{5/2} 4f_{5/2} J = 5/2)$				
(12)	Pd-like W^{28+}	nl, LSJ	$4d^9 4f\ ^1P_1$	$\rightarrow 4d^{10}\ ^1S_0$	48.91	48.948[b]	48.26	49.295[b]
		$(nl, jj$	$4d^3_{3/2} 4d^6_{5/2} 4f_{5/2} J = 1$	$4d^4_{3/2} 4d^6_{5/2} J = 0)$		48.9[a]		
(13)	Rh-like W^{29+}	nl, LSJ	$4d^8 4f\ ^2P_{3/2}$	$\rightarrow 4d^9\ ^2D_{5/2}$		49.938[d]	48.64	50.034[d]
		$(nl, jj$	$4d^3_{3/2} 4d^5_{5/2} 4f_{5/2} J = 3/2$	$4d^4_{3/2} 4d^5_{5/2} J = 5/2)$	49.34			
	Rh-like W^{29+}	nl, LSJ	$4d^8 4f\ ^2D_{5/2}$	$\rightarrow 4d^9\ ^2D_{5/2}$		50.265[d]	48.77	50.010[d]
		$(nl, jj$	$4d^4_{3/2} 4d^4_{5/2} 4f_{5/2} J = 5/2$	$4d^4_{3/2} 4d^5_{5/2} J = 5/2)$				

[a]Reference [22].
[b]Reference [23].
[c]Reference [24].
[d]Reference [25].

were identified comparing the experimental spectrum with the CR-model spectrum and from experimental appearance energy. The transitions and wavelengths of these emission lines are shown in Table II. This table also includes other experimental and calculated wavelengths [22–25]. Similar to the nl-$4l'$ transitions in the short-wavelength region, the emission lines of the $4l$-$4l'$ transitions from Ag-, Pd-, and Rh-like ions are very strong and sharp. These are due to simple electron configurations (Ag-like, Pd-like, and Rh-like ions) compared with other charge state ions. These sharp lines are also prominent even in the fusion and laser plasmas [2,22,26], which generally show broadbandlike emission from a wide charge state distribution. Therefore, these sharp and strong emission lines are possible to use for plasma diagnostics.

V. SUMMARY

We presented the measurements of the EUV spectra of highly charged tungsten ions in the wavelength range from 15 to 55 Å. From the electron energy dependence of experimental spectra, the emission lines of the $6g$-$4f$, $5g$-$4f$, $5f$-$4d$, $5p$-$4d$, and $4f$-$4d$ transitions were identified. The tungsten ion charge state dependence of these transition wavelengths and intensities was observed. We have constructed an original CR model for W^{19+}–W^{34+} ions, and these calculated spectra agree with experimental spectra of CoBIT. The $6g$-$4f$, $5g$-$4f$, $5f$-$4d$, $5p$-$4d$, and $4f$-$4d$ fine-structure transitions of Ag-like, Pd-like, and Ph-like tungsten ions were identified.

ACKNOWLEDGMENTS

This research was performed with the support and under the auspices of the NIFS Collaboration Research program (Grants No. NIFS09KOAJ003 and No. NIFS12KLPF024) and JSPS Grant-in-Aid for Scientific Research (A) (Grant No. 23246165) and (B) (Grant No. 22340175).

[1] T. Pütterich, R. Neu, C. Biedermann, R. Radtke, and ASDEX Upgrade Team, J. Phys. B: At., Mol. Opt. Phys. **38**, 3071 (2005).
[2] M. B. Chowdhuri, S. Morita, M. Goto, H. Nishimura, K. Nagai, and S. Fujioka, Plasma Fusion Res. **2**, S1060 (2007).
[3] J. Clementson, P. Beiersdorfer, E. W. Magee, H. S. McLean, and R. D. Wood, J. Phys. B: At., Mol. Opt. Phys. **43**, 144009 (2010).
[4] J. Clementson and P. Beiersdorfer, Phys. Rev. A **81**, 052509 (2010).
[5] Y. Ralchenko, J. Reader, J. M. Pomeroy, J. N. Tan, and J. D. Gillaspy, J. Phys. B: At., Mol. Opt. Phys. **40**, 3861 (2007).
[6] S. Wu and R. Hutton, Can. J. Phys. **86**, 125 (2008).
[7] Y. Podpaly, J. Clementson, P. Beiersdorfer, J. Williamson, G. V. Brown, and M. F. Gu, Phys. Rev. A **80**, 052504 (2009).
[8] N. Nakamura, H. Kikuchi, H. A. Sakaue, and T. Watanabe, Rev. Sci. Instrum. **79**, 063104 (2008).
[9] H. A. Sakaue, D. Kato, N. Nakamura, E. Watanabe, N. Yamamoto, and T. Watanabe, J. Phys.: Conf. Ser. **163**, 012020 (2009).
[10] A. Komatsu, J. Sakoda, N. Nakamura, H. A. Sakaue, X. Ding, D. Kato, I. Murakami, and F. Koike, Phys. Scr. **T144**, 014012 (2011).
[11] J. Yatsurugi, E. Watanabe, H. Ohashi, H. A. Sakaue, and N. Nakamura, Phys. Scr. **T144**, 014031 (2011).
[12] H. A. Sakaue, D. Kato, X. Ding, I. Murakami, F. Koike, T. Nakano, N. Yamamoto, H. Ohashi, J. Yatsurugi, and N. Nakamura, in *17th International Conference on Atomic Processes in Plasma*, edited by K. Aggarwal and F. Shearer, AIP Conf. Proc. No. 1438 (AIP, New York, 2012), pp. 91.
[13] A. Bar-Shalon, M. Klapisch, and J. Oreg, J. Quant. Spectrosc. Radiat. Transfer **71**, 169 (2001).
[14] A. E. Kramida and T. Shirai, At. Data Nucl. Data Tables **95**, 305 (2009).
[15] H. A. Sakaue, N. Yamamoto, S. Morita, N. Nakamura, C. Chen, D. Kato, H. Kikuchi, I. Murakami, S. Ohtani, H. Tanuma, T. Watanabe, and H. Tawara, J. Appl. Phys. **109**, 073304 (2011).
[16] U. I. Safronova, A. S. Safronova, P. Beiersdorfer, and W. R. Johnson, J. Phys. B: At., Mol. Opt. Phys. **44**, 035005 (2011).
[17] U. I. Safronova and A. S. Safronova, J. Phys. B: At., Mol. Opt. Phys. **43**, 074026 (2010).
[18] E. P. Ivanova, At. Data Nucl. Data Tables **95**, 786 (2009).
[19] C. S. Harte, T. Higashiguchi, T. Otsuka, R. D'Arcy, D. Kilbane, and G. O'Sullivan, J. Phys. B: At., Mol. Opt. Phys. **45**, 205002 (2012).
[20] R. D. Cowan, *The Theory of Atomic Structure and Spectra* (University of California Press, Berkeley, 1991).
[21] S. Morita, C. F. Dong, M. Goto, D. Kato, I. Murakami, H. A. Sakaue, M. Hasuo, F. Koike, N. Nakamura, T. Oishi, A. Sasaki, and E. H. Wang, in *Eighth International Conference on Atomic and Molecular Data and Their Applications*, edited by J. D. Gillaspy, W. L. Wiese, and Y. A. Podpaly, AIP Conf. Proc. No. 1545 (AIP, New York, 2013), pp. 143.
[22] K. Asmussen, K. B. Fournier, J. M. Laming, R. Neu, J. F. Seely, R. Dux, W. Engelhardt, and J. C. Fuchs, Nucl. Fusion **38**, 967 (1998).
[23] J. Sugar, V. Kaufman, and W. L. Rowan, J. Opt. Soc. Am. B **10**, 799 (1993).
[24] J. Sugar, V. Kaufman, and W. L. Rowan, J. Opt. Soc. Am. B **10**, 1321 (1993).
[25] J. Sugar, V. Kaufman, and W. L. Rowan, J. Opt. Soc. Am. B **10**, 1977 (1993).
[26] C. Suzuki, T. Kato, H. A. Sakaue, D. Kato, K. Sato, N. Tamura, S. Sudo, N. Yamamoto, H. Tanuma, H. Ohashi, R. D'Arcy and G. O'Sullivan, J. Phys. B: At., Mol. Opt. Phys. **43**, 074027 (2010).